metals

Article

Effect of Basketweave Microstructure on Very High Cycle Fatigue Behavior of TC21 Titanium Alloy

Baohua Nie [1], Zihua Zhao [2,*], Dongchu Chen [1], Shu Liu [1], Minsha Lu [1], Jianglong Zhang [2] and Fangming Liang [1]

1 School of Materials Science and Energy Engineering, Foshan University, Foshan 528000, China; niebaohua121@163.com (B.N.); chendc@fosu.edu.cn (D.C.); liushu814194678@126.com (S.L.); wyffhpwzy@163.com (M.L.); lfm314469592@163.com (F.L.)
2 School of Materials Science and Engineering, Beihang University, Beijing 100191, China; zhangjl1330@buaa.edu.cn
* Correspondence: zhzh@buaa.edu.cn; Tel.: +86-010-8231-3264

Received: 1 May 2018; Accepted: 29 May 2018; Published: 30 May 2018

Abstract: This paper discusses the effect of basketweave microstructure on the very high cycle fatigue behavior of TC21 titanium alloy. Ultrasonic fatigue tests at 20 kHz are done on a very high cycle fatigue (VHCF) property of the alloys with 60 μm and 40 μm basketweave size, respectively. Results show that the alloys illustrate step-wise S-N characteristics over the 10^5–10^9 cycle regimes and that fatigue fracture in both of the alloys occur beyond the conventional fatigue limit of 10^7 cycles. Subsurface crack initiation occurs at low stress amplitude. A fine granular area (FGA) is observed along the α lamella at the subsurface crack initiation site. The mechanism for the subsurface crack initiation is revealed using layer-by-layer-polishing, due to the micro-voids that are introduced at the granular α phase. The colony of α lamella is due to the local stress concentrated between them under the cyclic load. The stress intensity factor range at the FGA front is regarded as the threshold value controlling the internal crack propagation. Furthermore, the effect of the baseketweave size on the very high cycle fatigue limits of the TC21 titanium alloy is evaluated based on the Murakami model, which is consistent with the experimental results. The fatigue life of TC21 titanium alloy is well predicted using the energy-based crack nucleation life model.

Keywords: very high cycle fatigue; crack initiation; titanium alloy; basketweave microstructure

1. Introduction

High strength titanium alloys are usually used in aeronautical force-bearing components as a result of their high specific strength and excellent corrosion properties [1]. Throughout their ultra-long time service, the components are subjected to cyclic load with high frequency and low amplitude, thus the very high cycle fatigue (VHCF) of titanium alloy has been drawing world wide attention [2,3]. Fatigue failure in high strength titanium alloys occurs beyond the conventional fatigue limit of 10^7 cycles, and the stress-number of cycles to failure (S-N) curves exhibit a step-wise shape [2] or a decreasing shape [4]. Another important characteristic of these titanium alloys is that the crack initiation site shifts from the surface-induced fracture at low cycle regimes to a subsurface-induced fracture at very high cycle regimes [5], which may be responsible for the variability of the fatigue properties and the step-wise shape of the S-N curve. Thus, it is hazardous to design aeronautical components based on conventional fatigue strength data.

Obviously, the microstructure of the titanium alloys significantly affects the fatigue properties and the fatigue crack initiation mechanisms in a very high cycle regime. As for titanium alloys with a bimodal microstructure, α grain size [6–8], grain distribution [9], crystal orientation [10,11], and super grain (grain clusters with similar orientation) [12] are important factors of the fatigue crack initiation for titanium alloys. The mechanism of the fine granular area (FGA) was supposed to be the cleavage of primary α grains, followed by the growth and coalescence of the adjacent facets [5,13,14]. The probabilities of faceted crack initiation increase with the value of the stress ratio R (the ratio of the min stress to the max stress), and the rough area, other than the facets characteristics, were observed at the stress ratio of −1 [13]. The formation of a rough area at the ratio of −1 was explained based on the numerous cyclic pressing (NCP) model [14].

However, till now the fracture mechanism and fatigue properties in a very high cycle regime for the titanium alloys basketweave microstructure has not been very well understood. V. Crupi et al. [15] investigated the very high cycle fatigue behavior of Ti6Al4V alloy with both bimodal and lamellar microstructures. The alloy with lamellar microstructure had fatigue strength lower than that with bimodal microstructure, and the crack initiated from the surface without subsurface facets. The investigation by Zuo et al. [5] indicated a very high cycle fatigue crack initiated from α/β interfaces in Ti6Al4V with lamellar microstructure due to the dislocation arrays pile-up at α/β interfaces, where the crack initiation site displayed flat facet characteristics. It is noted that α/β lamellar played an important role in the very high cycle fatigue crack initiation, but the effect of granular α phase, which is a typical microstructure at the grain boundary, has been ignored.

TC21 alloy is an α + β titanium alloy usually used in aeronautical force-bearing components due to its fatigue damage tolerance, excellent welding, and formation performance [1]. The VHCF behavior of TC21 titanium alloy with basketweave microstrucutrue was investigated in the present work. A fatigue crack initiation mechanism is revealed using the layer-by-layer-polishing approach to observe the microstructure as well as the defects underneath the crack initiation site. The effect of basketweave on fatigue strength and initiation life is quantitatively estimated based on the fatigue fracture theory.

2. Experimental Procedures

2.1. Materials

The material used in this study was TC21 titanium alloy with a nominal chemical composition of Ti-6Al-2Sn-2Zr-3Mo-1Cr-2Nb. The alloy was forged at 940 °C with deformation ratio up to 50%, 80%, air quenching, following as 900 °C for 2 h + air quenching, and then 600 °C for 4 h + air quenching. The thermo-mechanical treatment procedures had basketweave microstrucrture with the mean sizes of 60 and 40 μm, and the granular α phase was observed in both samples (Figure 1a,b). Furthermore, a double lamellar basketweave microstructure, where secondary α lamella was present in β lamella, can be observed in the alloys, as shown in Figure 1c. The alloys with the basekweave size of 60 and 40 μm obtained a high tensile strength of 1070 MPa, 1100 MPa, respectively.

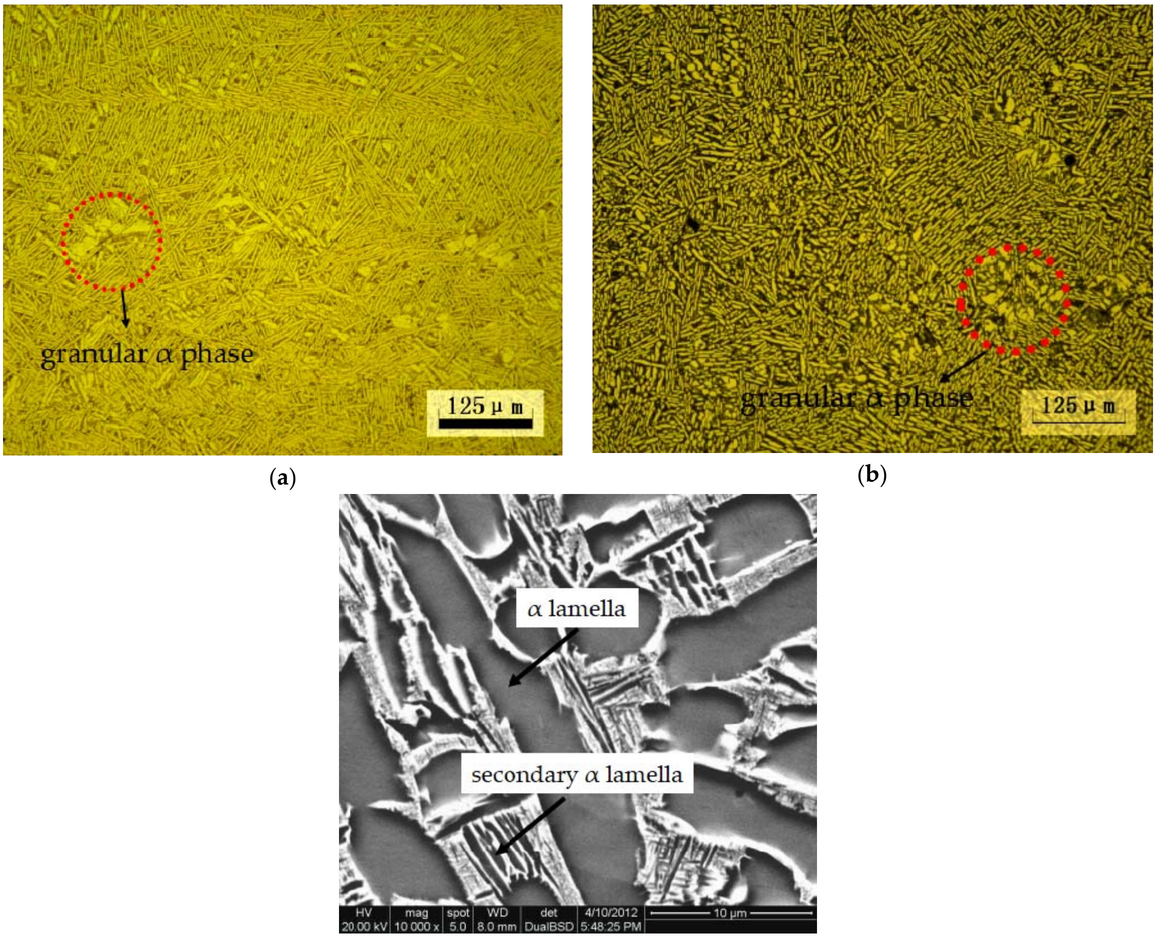

(**a**) (**b**)

(**c**)

Figure 1. Basketweave microstructures of TC21 titanium alloy: (**a**) basketweave size of 60 μm (OM); (**b**) basketweave size of 40 μm (OM) and (**c**) a double lamellar basketweave microstructure (SEM).

2.2. Surface Treatment

The specimens underwent electro-polishing (EP) to remove the machining layers to observe the fatigue damage morphology and eliminate its influence on fatigue behavior. Electro-polishing was carried out in 59% methanol, 35% n-butanol, 6% perchloric acid under −20 °C, and 20–25 V voltage.

2.3. Ultrasonic Fatigue Test

Fatigue tests were carried out using an ultrasonic fatigue test machine (20 kHz, SHIMADZU, Kyoto, Japan) at a constant stress ratio of −1. This method is an accelerated testing method with a frequency far beyond that of the conventional fatigue experiments. The frequency effect is small for ultrasonic fatigue tests under low displacement and small deformation [16]. Very high cycle fatigue behaviors of many metallic materials have been investigated using an ultrasonic fatigue test machine, which includes an ultrasonic generator, a piezoelectric converter, an ultrasonic horn, and a computer control system [17]. An ultrasonic generator transforms 50 or 60 Hz voltage signals into sinusoidal signals with 20 kHz; a piezoelectric converter excited by the generator transforms the electrical signal into a longitudinal mechanical vibration with the same frequency; an ultrasonic horn amplifies the vibration displacement in order to obtain the required strain amplitude in the middle section of the specimen; a computer control system is necessary to control the load amplitude and acquire the test data. The maximum displacement amplitude measured by a dynamic sensor is obtained at the end of the specimen while the strain excitation in the push-pull cycles (load ratio $R = -1$) reaches the maximum in the middle section of the specimen, which produces the required high frequency fatigue stress. In addition, a compressed air cooling gun is necessary to prevent the temperature from increasing during the tests.

Considering that the amplifier and the specimen must work at resonance, the specimen geometry was designed using the elastic wave theory. Figure 2 shows the geometries of the fatigue specimens and its dimensions.

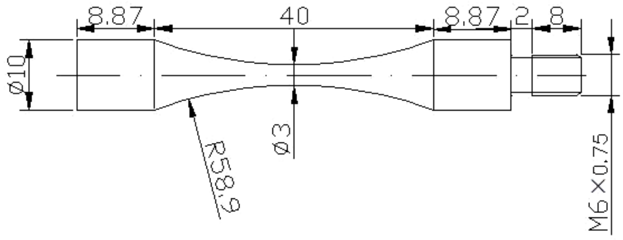

Figure 2. Shape and dimensions of the test specimens (unit: mm).

2.4. Observation of Microstructure at the Crack Initiation Site

In order to investigate the fatigue crack initiation mechanism of the TC21 titanium alloy, the microstructure characteristic at crack initiation site was observed. As for the surface crack initiation, the fracture surface was protected by the resin, then the side of the crack initiation site was etched. The resin was removed by the acetone and the microstructure characteristic of the surface crack origin was observed by the tilt function of the scanning electron microscope (Hitachi Limited, Tokyo, Japan) for subsurface crack initiation specimens, the fatigue fracture was embedded with the resin, and the exact location of the crack initiation site was marked by the coordinate method. The microstructure at the subsurface crack initiation site was observed using the layer-by-layer polishing method.

3. Results and Discussion

3.1. S-N Characteristics

Step-wise characteristics can be observed on the S-N curve over the wide range of the 10^5–10^9 cycle regimes for the TC21 titanium alloy with two sizes of basketweave (Figure 3). Fatigue fracture in both alloys occurs beyond the conventional fatigue limit of 10^7 cycles but present very high cycle fatigue limits with 530 and 430 MPa, respectively. Step-wise characteristics can be also observed in the VHCF of the TC4 titanium alloy with bimodal microstructure [18], however, the research by Zuo [5] has shown that the the S-N curve of Ti6Al4V with basketweave decreased continuously and turns less sharply at about 5×10^7 cycles, and there exists no horizontal asymptote and fatigue limit, which could result from the different basketweave sizes. Figure 3 also shows fatigue properties of the alloy with basketweave of 40 μm are higher than that of 60 μm, although these two specimens have a similar tensile strength. It is can be attributed to the shorter effective slip length for the specimens with fine basketweave [19].

The step-wise characteristics can be the results of the shift of crack initiation mechanism. Based on SEM observation of all fracture surfaces, for both kinds of alloys, the fatigue cracks initiate from the sample's surface at relatively high stress amplitudes, whereas the crack initiation mode shifts to the subsurface with a fine granular area (FGA) initiation model at approximately 600 and 540 MPa over the wide range of 10^5 to 10^7 cycle regimes. The crack initiation mechanisms for the surface and subsurface initiation models are discussed below.

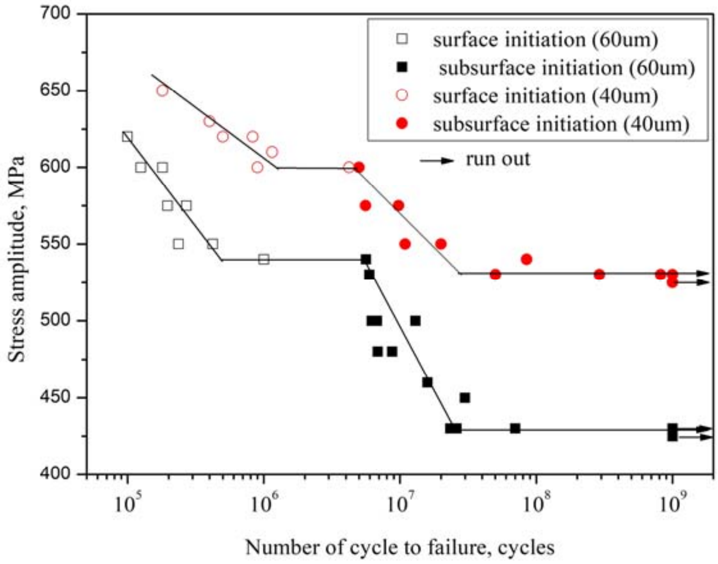

Figure 3. S-N curve of TC21 titanium alloy with two sizes of basketweave.

3.2. Fatigue Crack Initiation Analysis

The typical surfaces initiation of the TC21 titanium alloy with basketweave of 60 μm and 40 μm are shown in Figure 4. Fatigue crack is initiated from the sample surface under high stress amplitude and a radial ridge pattern parallel to the crack propagation direction is observed on the fracture surface. However, fatigue crack under low stress amplitude initiates from the sample subsurface (Figures 5 and 6). α/β lamellar characteristics are present at the crack initiation site where the fine granular is distributed on α lamella and FGA has the same size as the colony of lamella (Figure 5). The similar rough area characteristic at the crack initiation site is often observed in bidomal equiaxed microstructure at $R = -1$, which was explained based on the numerous cyclic pressing (NCP) model [14]. The probability of rough area at the crack initiation site is decreased with the increase of the stress ratio of −1 [13]. As for TC21 titanium alloy with basketweave of 40 μm, the fracture surfaces are similar to that of the alloy with basketweave of 60 μm. Fatigue crack initiates shifts from the sample surface to the subsurface under a low stress amplitude (Figure 6), however, α/β lamella characteristics are insignificant at the crack initiation site probably because of the small size of the α/β lamella.

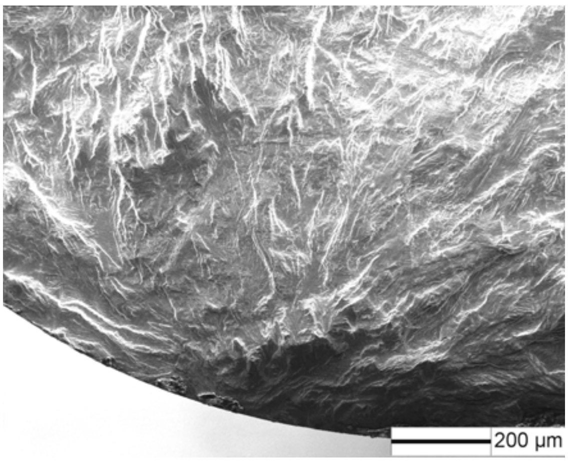

(**a**)

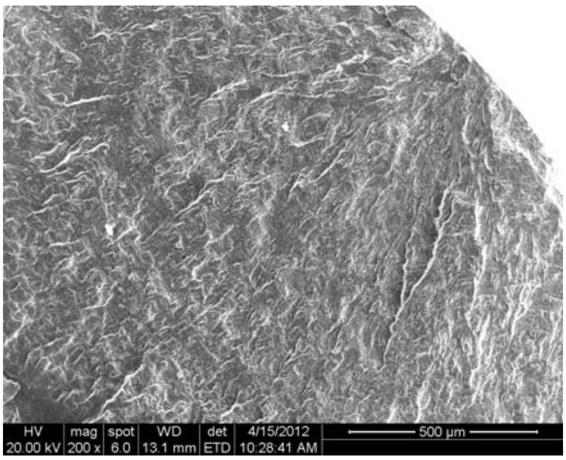

(**b**)

Figure 4. Fatigue fracture surface of TC21 titanium alloy: (**a**) basketweave of 60 μm at σ = 550 MPa, $N = 2.37 \times 10^5$ cycles; (**b**) basketweave of 40 μm at σ = 610 MPa, $N = 1.15 \times 10^6$ cycles.

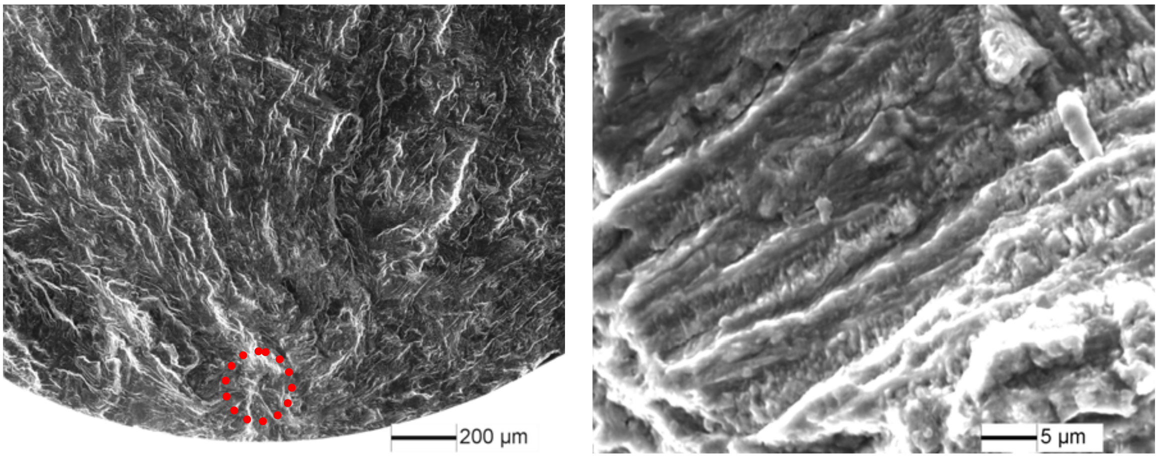

(**a**) (**b**)

Figure 5. Fatigue fracture surface of TC21 titanium alloy with basketweave of 60 μm at σ = 500 MPa, $N = 6.66 \times 10^6$ cycles: (**a**) fatigue crack initiation site; (**b**) high magnification morphology.

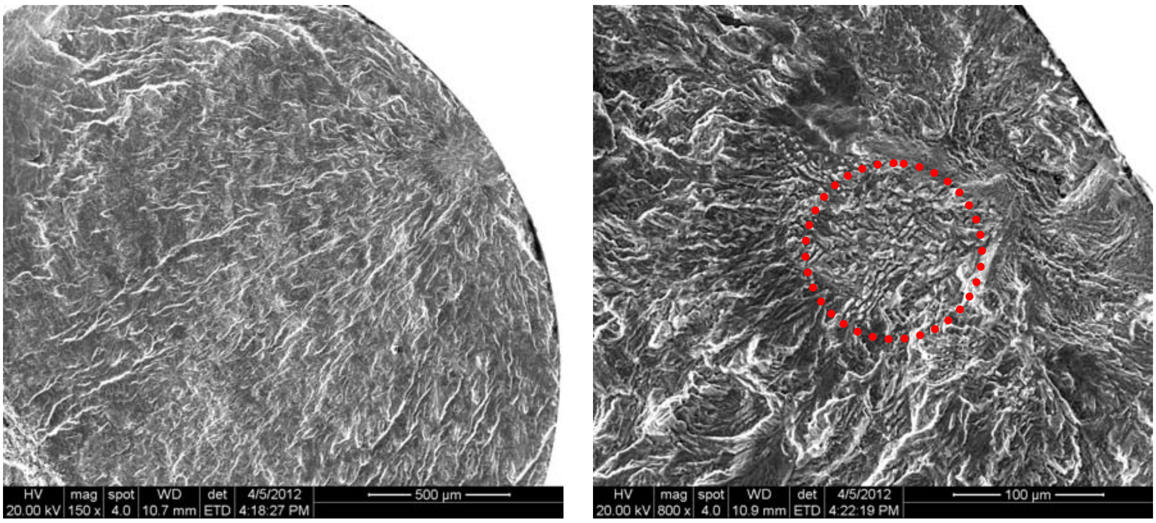

(**a**) (**b**)

Figure 6. Fatigue fracture surface of TC21 titanium alloy with basketweave of 40 μm at σ = 540 MPa, $N = 8.51 \times 10^7$ cycles: (**a**) fatigue crack initiation site; (**b**) high magnification morphology.

The microstructure of the surface crack initiation site can be observed by SEM due to the surface electro-polishing treatment shown in Figure 7. It is obvious that the surface crack initiates at α/β interface at a high stress amplitude. The priority deformation of α phase occurs under cyclic load, and the dislocation concentrates at the α/β interface producing severe local stress concentration. Thus, α/β interface becomes preferential crack initiation sites in a high cycle regime, even in a very high cycle regime [15].

FGA is present at the subsurface initiation site for the TC21 alloy, which has no inclusions or porosities. The subsurface initiation of cracks is associated with the microstructural inhomogeneity. The microstructure at the subsurface crack initiation site is observed using the layer-by-layer polishing method. Observation of the subsurface microstructure shows that some micro-voids are distributed in α lamella in the vicinity of the coarse granular α phase (Figure 7). It is speculated that nanocracks can propagate by linkage with the micro-voids in front of the crack tip by cyclic loading without much plasticity [20]. Taking Figure 6 as an example, the FGA radius is approximately 42 μm under 8.51×10^7 loading cycles. Considering that most of the fatigue life is spent in the FGA crack propagation [21,22], the average fatigue crack growth rate is approximately 4.9×10^{-13} m/cycle, which is lower than the lattice spacing and thereby indicates that the fatigue crack cannot propagate cycle-by-cycle.

Figure 7 suggests that the micro-plasticity damage occurs due to the local microstructural inhomogeneity. As a result of the severe local stress concentrated at the interface between the granular α phase and the colony of α/β lamellae under cyclic load, a microcrack is formed in the granular α phase due to priority deformation, and nanograin layers at the microcrack wake are produced by the repeated pressing between the crack surfaces along the α lamella [14]. Micro-voids can be introduced at the nanograin boundary, then the coalescence and linkage of the micro-voids results in the separation of the nanograin layer, which displays FGA characteristics. The crack initiation at α lamella is also reported in very high cycle fatigue of Ti6Al4V, however, the flat facets were displayed on the lamella [5], which may be owing to the absence of the granular α phase in the alloy. The α/β lamellae interface is the weak link for crack initiation, causing a cleavage on the plane with a favorable orientation because of the restricted operative slip systems.

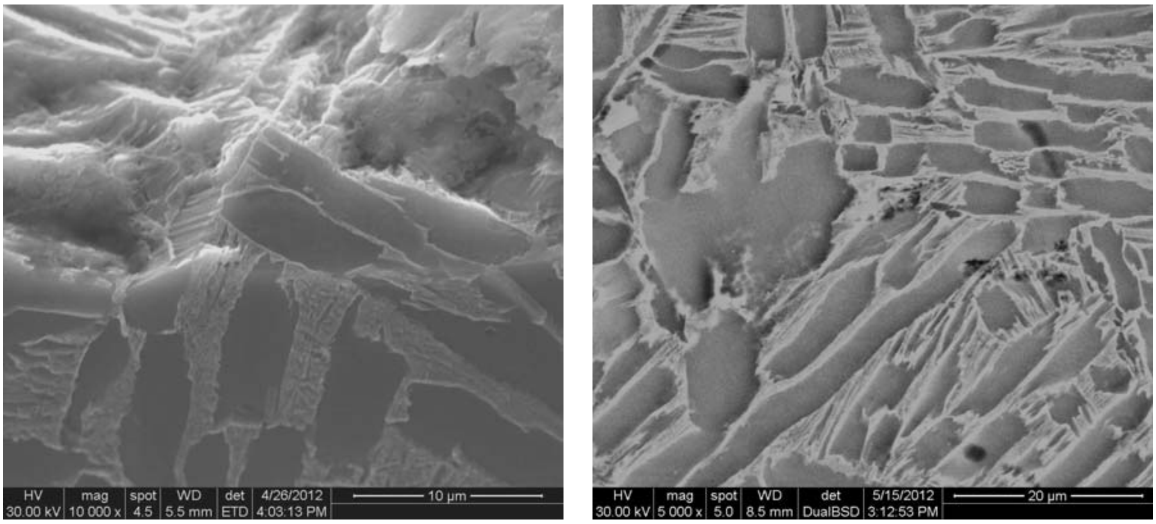

(**a**) (**b**)

Figure 7. Fatigue crack initiation and microstructure characteristics with basketweave of 40 µm: (**a**) surface initiation, σ = 610 MPa, $N = 1.15 \times 10^6$ cycles; (**b**) subsurface initiation, σ = 540 MPa, $N = 8.51 \times 10^7$ cycles.

3.3. Effect of Basketweave on Fatigue Fracture Mechanism

For the subsurface fracture model, the initial stress intensity factor range at the FGA front can be calculated using the Murakami model [23]:

$$\Delta K_{FGA} = 0.5\sigma_a\sqrt{\pi\sqrt{area_{FGA}}} \quad (1)$$

where σ_a is the stress amplitude and $area_{FGA}$ is the area of FGA at the crack origin. In ultrasonic fatigue with a mean load equal to zero ($R = -1$), only the tensile part of the cycle has a predominant effect on the fatigue crack propagation [24]. Thus, ΔK_{FGA} is calculated by substituting σ_a into Equation (1) instead of $\Delta\sigma$.

The relationship between the stress intensity factor range at FGA and fatigue life is shown in Figure 8. The alloy with basketweave of 60 µm and 40 µm have the same of ΔK_{FGA} value, which has a scattering zone ranging from 3.8 MPa·m$^{1/2}$ to 4.5 MPa·m$^{1/2}$ (Figure 8), and can be considered as the threshold for the crack growth ΔK_{th} [24]. Zhao et al. [25] supposed that the growth of FGA was restricted by the related microstructure, and the FGA crack cannot propagate when the plastic zone size ahead of the FGA crack tip is equal to the characteristic dimension of the materials. Thus, the value of ΔK_{FGA} can be evaluated as [26]:

$$\Delta K_{FGA} = 4.342\mu\sqrt{b} \tag{2}$$

Equation (2) implies that ΔK_{FGA} is a function of the shear modulus μ and the Burgers vector *b* of materials. According to Equation (2), the value of ΔK_{FGA} is about 3.54 MPa·m$^{1/2}$ for TC21 alloy, which is consistent with various experimental results of 3.4–4.0 MPa·m$^{1/2}$ [26,27], but slightly lower than this experiment data.

As for subsurface crack initiation, FGA is found along the basketweave (Figures 5 and 6), indicating the significant effect of basketweave on the hindering of FGA. Chapetti [28] assumed that the strongest microstructure was the barrier for fatigue crack propagation at the critical nominal stress range needed for a continued crack growth (microstructural threshold). Fatigue crack is assumed to be hindered at the first basketweave under very high cycle fatigue limit stress; the FGA area can be treated as a circular area with a radius equal to basketweave. From Equation (1), a very high cycle fatigue limit of titanium alloy with basketweave microstructure can be expressed as

$$\sigma_a = \frac{2\Delta K_{FGA}}{\sqrt{\pi\sqrt{area_{FGA}}}} = \frac{2\Delta K_{th}}{\sqrt{\pi\sqrt{area_{\alpha/\beta}}}} \tag{3}$$

The typical ΔK_{th} for the alloy with basketweave of 60 and 40 μm are 4 MPa·m$^{1/2}$. The very high cycle fatigue limit for the alloy with basketweave of 60 and 40 μm are 438 and 536 MPa based on Equation (3), which are consistent with the experimental results. Therefore, basketweave size remarkably affects the very high cycle fatigue properties of the TC21 titanium alloy and is responsible for the variability of fatigue properties.

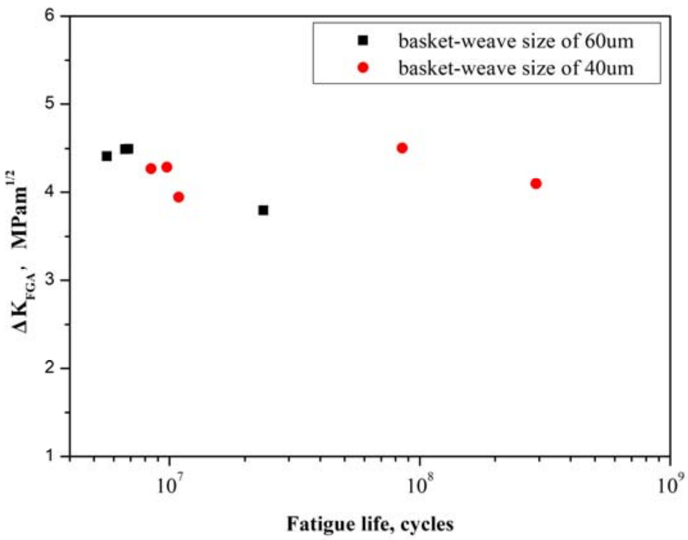

Figure 8. Relationship between the stress intensity factor range at FGA and fatigue life.

3.4. Effect of Basketweave on Fatigue Life

Considering that most of the total VHCF fatigue life is consumed by the crack initiation stage, fatigue life of TC21 alloy can be estimated using an energy-based crack nucleation life model, which can be calculated as [17]:

$$N_i = \frac{4\pi\mu^3 h^2 M^3 c}{0.005 d^3 (\Delta\sigma - 2Mk)[\pi^2\Delta\sigma^2(1-v)^2 + \xi M^2\mu^2]} \tag{4}$$

where $\Delta\sigma$ is the stress amplitude for the stress ratio of -1. μ, ν are the shear modulus and Poisson's ratio of material, d is the microstructure characteristics size, and it is the size of basketweave in this paper, c is the size of crack, which is herein considered as the size of FGA, M is the Taylor factor and is equal to 2, $2Mk$ is the fatigue limit defined as the fatigue strength at the life of 10^9 cycles, parameters h and ξ can be determined by the fitting of the S-N curves, and then the nucleation life curves for different microstructure can be established.

Based on the fatigue data of TC21 alloy with basketweave microstructure, parameters h and ξ are fitted as 0.9 and 0.0001, and the prediction of the subsurface crack nucleation life is shown in Figure 9. It is suggested that the energy-based crack nucleation life model can be well used to predict the subsurface crack nucleation life, and the large basketweave size significantly reduces the fatigue life. Thus, fatigue properties can be improved by the refinement of basketweave.

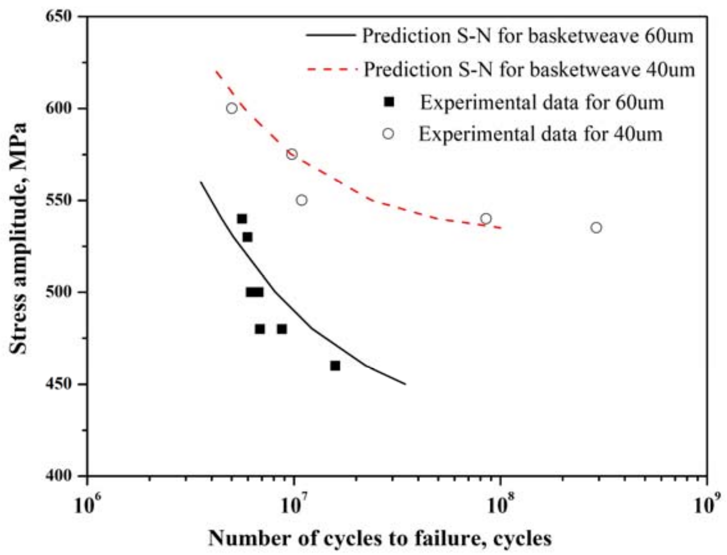

Figure 9. Comparison of the predicted fatigue life with different basketweave size versus the experimental data.

4. Conclusions

The conclusions are summarized as follows:

(1) Step-wise S-N characteristics are observed on a TC21 titanium alloy with two sizes of basketweave over 10^5–10^9 cycle regimes. The fatigue property of the alloy with basketweave of 40 μm is higher than that of 60 μm.

(2) Fatigue crack initiates from the surface α/β phase interface at a relatively high stress amplitude, whereas the fatigue crack site appears at the sample subsurface at a relatively low stress amplitude; α/β lamellar characteristic is present at the crack initiation site of the alloy where FGA is found alongside basketweave.

(3) Very high cycle fatigue limits of TC21 titanium alloy with basketweave microstructure are evaluated based on the Murakami model, which are consistent with the experimental results. The fatigue life of TC21 titanium alloy is well predicted using tan energy-based crack nucleation life model.

Author Contributions: Z.Z. and D.C. conceived and designed the experiments; J.Z., M.L., F.L. and S.L. performed the experiments; B.N. analyzed the experiments, and wrote the paper.

Funding: This work was supported by the National Natural Science Foundation of China (Grant No. 51571009). Special funds for the scientific and technological development of Guangdong (2017A010103029). Foshan programs of science and technology research (2017AB003941), the "5511" project driven innovation program of Yichun City, the talent research start-up program of Foshan University (gg040940).

Conflicts of Interest: The authors declare no conflict of interest.

References

1. Zheng, Y.; Zhao, Z.H.; Zhang, Z.; Zong, W.; Dong, C. Internal crack initiation characteristics and early growth behaviors for very-high-cycle fatigue of a titanium alloy electron beam welded joints. *Mater. Sci. Eng. A* **2017**, *706*, 311–318. [CrossRef]
2. Nie, B.; Zhao, Z.; Ouyang, Y.; Chen, D.; Chen, H.; Sun, H.; Liu, S. Effect of low cycle fatigue predamage on very high cycle fatigue behavior of TC21 titanium alloy. *Materials* **2017**, *10*, 1384. [CrossRef] [PubMed]
3. Nie, B.; Zhao, Z.; Liu, S.; Chen, D.; Ouyang, Y.; Chen, H.; Fan, T.; Sun, H. Very high cycle fatigue behavior of a directionally solidified Ni-base superalloy DZ4. *Materials* **2018**, *11*, 98. [CrossRef] [PubMed]
4. Wu, Y.; Liu, J.R.; Wang, H.; Guan, S.X.; Yang, R.; Xiang, H.F. Effect of stress ratio on very high cycle fatigue properties of Ti-10V-2FE-3Al alloy with duplex microstructure. *J. Mater. Sci. Technol.* **2017**. [CrossRef]
5. Zuo, J.H.; Wang, Z.G.; Han, E.H. Effect of microstructure on ultra-high cycle fatigue behavior of Ti-6Al-4V. *Mater. Sci. Eng. A* **2008**, *473*, 147–152. [CrossRef]
6. Sushant, K.J.; Christopher, J.S.; Patrick, J.G.; William, J.P.; Reji, J. Characterization of fatigue crack-initiation facets in relation to lifetime variability in Ti-6Al-4V. *Int. J. Fatigue* **2012**, *42*, 248–257.
7. McEvily, A.J.; Nakamura, T.; Oguma, H.; Yamashita, K.; Matsumnaga, H.; Endo, M. On the mechanism of very high cycle fatigue in Ti-6Al-4V. *Scr. Mater.* **2008**, *59*, 1207–1209. [CrossRef]
8. Oguma, H.; Nakamura, T. The effect of microstructure on very high cycle fatigue properties in Ti-6AL-4V. *Scr. Mater.* **2010**, *63*, 32–34. [CrossRef]
9. Szczepanski, C.J.; Jha, S.K.; Larsen, J.M.; Jones, J.W. Microstructural influences on very-high-cycle fatigue-crack initiation in Ti-6246. *Metall. Mater. Trans. A* **2008**, *39*, 2841–2851. [CrossRef]
10. LeBiavant, K.; Pommier, S.; Prioul, C. Local texture and fatigue crack initiaton in a Ti-6Al-4V. *Fatigue Fract. Eng. Mater. Struct.* **2002**, *25*, 527–545. [CrossRef]
11. Sinha, V.; Spowart, J.E.; Mills, M.J.; Williams, J.C. Observations on the faceted initiation site in the dwell-fatigue tested Ti-6242 alloy: Crystallographic orientation and size effects. *Metall. Mater. Trans. A* **2006**, *37*, 1507–1518. [CrossRef]
12. Ravi Chandran, K.S.; Jha, S.K. Duality of the S-N fatigue curve caused by competing failure modes in a titanium alloy and the role of Poisson defect statistics. *Acta Mater.* **200**, *53*, 1867–1881. [CrossRef]
13. Liu, X.L.; Sun, C.Q.; Hong, Y.S. Faceted crack initiation characteristics for high-cycle and very-high-cycle fatigue of a titanium alloy under different stress ratios. *Int. J. Fatigue* **2016**, *92*, 434–441. [CrossRef]
14. Pan, X.; Su, H.; Sun, C.; Hong, Y. The behavior of crack initiation and early growth in high-cycle and very high-cycle fatigue regimes for a titanium alloy. *Int. J. Fatigue* **2018**. [CrossRef]
15. Crupi, V.; Epasto, G.; Guglielmino, E.; Squillace, A. Influence of microstructure [alpha + beta and beta] on very high cycle fatigue behaviour of Ti-6Al-4V alloy. *Int. J. Fatigue* **2017**, *95*, 64–75. [CrossRef]
16. Yang, K.; He, C.; Huang, Q.; Huang, Z.Y.; Wang, C.; Wang, Q.Y.; Liu, Y.L.; Zhong, B. Very high cycle fatigue behaviors of a turbine engine blade alloy at various stress ratios. *Int. J. Fatigue* **2017**, *99*, 35–43. [CrossRef]
17. Bathias, C. Piezoelectric fatigue testing machines and devices. *Int. J. Fatigue* **2006**, *28*, 1438–1445. [CrossRef]
18. Li, W.; Zhao, H.Q.; Nehila, A.; Zhang, Z.Y.; Sakai, T. Very high cycle fatigue of TC4 titanium alloy under variable stress ratio: Failure mechanism and life prediction. *Int. J. Fatigue* **2017**, *10*, 342–354. [CrossRef]
19. Zhang, S.Z.; Zeng, W.D.; Zhao, Q.Y.; Gao, X.X.; Wang, Q.J. High cycle fatigue of isothermally forged Ti-6.5Al-2.2Mo-2.2Zr-1.8Sn-0.7W-0.2Si with different microstructures. *J. Alloys Compd.* **2016**, *689*, 114–122. [CrossRef]
20. Horstemeyer, M.F.; Farkas, D.; Kim, S.; Tang, T.; Potirniche, G. Nanostructurally small cracks (NSC): A review on atomistic modeling of fatigue. *Int. J. Fatigue* **2010**, *32*, 1273–1502. [CrossRef]
21. Ranc, N.; Wagner, D.; Paris, P.C. Study of thermal effects associated with crack propagation during very high cycle fatigue tests. *Acta Mater.* **2008**, *56*, 4012–4021. [CrossRef]
22. Wang, Q.Y.; Bathias, C.; Kawagoishi, N.; Kawagoishi, N.; Chen, Q. Effect of inclusion on subsurface crack initiation and gigacycle fatigue strength. *Int. J. Fatigue* **2002**, *24*, 1269–1274. [CrossRef]
23. Murakami, Y.; Endo, M. Effects of defects, inclusion and inhomogeneities on fatigue strength. *Int. J. Fatigue* **1994**, *16*, 163–182. [CrossRef]

24. Nie, B.H.; Zhang, Z.; Zhao, Z.H.; Zhong, Q.P. Very high cycle fatigue behavior of shot peening 3Cr13 high strength spring steel. *Mater. Des.* **2013**, *50*, 503–508. [CrossRef]
25. Zhao, A.; Xie, J.; Sun, C.; Hong, Y. Prediction of threshold value for FGA formation. *Mater. Sci. Eng. A* **2011**, *528*, 6872–6877. [CrossRef]
26. Richie, R.O.; Davidson, D.L.; Boyce, B.L.; Campbell, J.P.; Roder, O. High-cycle fatigue of Ti6Al4V. *Fatigue Fract. Eng. Mater. Struct.* **1999**, *22*, 621–631.
27. Petit, J.; Sarrazin-Baudoux, C. An overview on the influence of the atmosphere environment on ultra-high-cycle fatigue and ultr-slow fatigue crack propagation. *Int. J. Fatigue* **2006**, *28*, 1471–1478. [CrossRef]
28. Chapetti, M.D. Fatigue assessment using an integrated threshold curve method-applications. *Eng. Fract. Mech.* **2008**, *75*, 1854–1863. [CrossRef]